PAPER

Engineering of a Pluronic F127 functionalized magnetite/graphene nanohybrid for chemophototherapy

To cite this article: Yongyong Li *et al* 2014 *Nanotechnology* **25** 065602

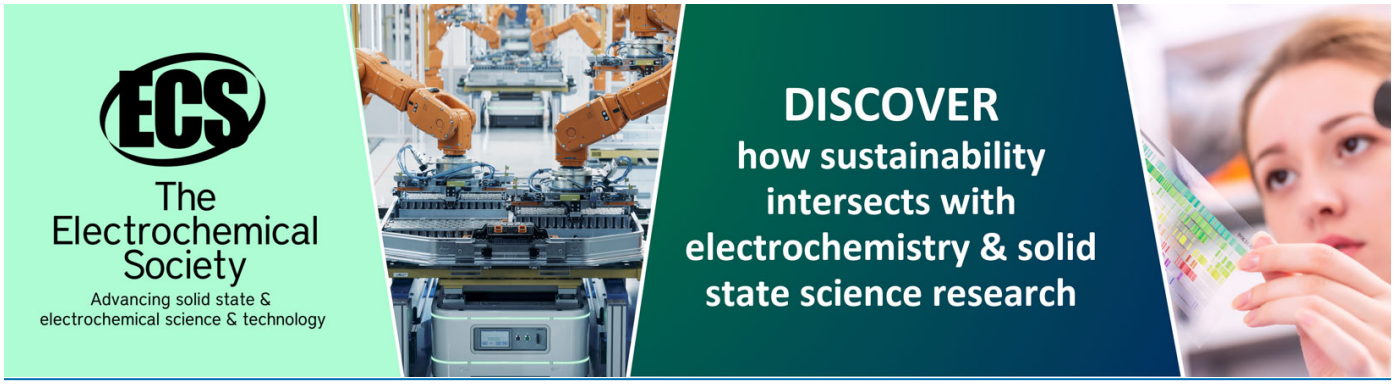

IOP Publishing Nanotechnology
Nanotechnology **25** (2014) 065602 (9pp) doi:10.1088/0957-4484/25/6/065602

Engineering of a Pluronic F127 functionalized magnetite/graphene nanohybrid for chemophototherapy

Yongyong Li[1], Jiaqiang Liu[2], Haiqing Dong[1], Guangzhen Liu[1] and Haiqing Hu[2]

[1] The Institute for Biomedical Engineering and Nano Science, Tongji University School of Medicine, Shanghai 200092, People's Republic of China
[2] School of Polymer Science and Engineering, Qingdao University of Science and Technology, Qingdao 266042, People's Republic of China

E-mail: yongyong_li@tongji.edu.cn and inano_donghq@tongji.edu.cn

Received 8 October 2013, revised 19 November 2013
Accepted for publication 25 November 2013
Published 16 January 2014

Abstract

In this study, a multifunctional graphene based nanohybrid, termed as GN/Fe_3O_4/PF127, is engineered via a facile one-pot process consisting of simultaneous reduction of graphene oxide/Fe_3O_4 and subsequent assembly of Pluronic F127 (PF127) onto graphene nanosheets (GNs). The unique aromatic and planar structure of GNs allows the attachment of multiple functional components including MRI contrast agent (Fe_3O_4 nanoparticles) and an aromatic anticancer drug like doxorubicin (DOX), as well as PF127 coating which imparts physiological dispersivity and stability to the nanohybrid. The successful assembly process is revealed by TEM observation, size and FITR monitoring. In contrast with the primitive graphene or its oxide derivative, the resulting GN/Fe_3O_4/PF127 nanohybrids have shown high biological dispersion and MRI effect for diagnosis due to the incorporation of superparamagnetic Fe_3O_4 nanoparticles without evident cytotoxicity. Moreover, the GN/Fe_3O_4/PF127 nanohybrid exhibits a photothermal effect due to the considerable optical absorption in the near-infrared region of GNs. The GN/Fe_3O_4/PF127 nanohybrid could be a further platform for chemophototherapy assisted by the therapeutic DOX. Cellular toxicity assays indicated that the DOX-loaded GN/Fe_3O_4/PF127 nanohybrid showed a remarkable cytotoxicity to HeLa cells and the cytotoxic effect was intensified when subjected to photoirradiation. Confocal laser scanning microscopy (CLSM) and flow cytometric analysis (FCAS) revealed that the nanohybrid could be easily uptaken into HeLa cells.

Keywords: graphene, Pluronic F127, Fe_3O_4, nanohybrid, chemophototherapy

S Online supplementary data available from stacks.iop.org/Nano/25/065602/mmedia

(Some figures may appear in colour only in the online journal)

1. Introduction

Graphene, a bright star in materials science, has attracted intensive and extensive attention due to its unique physical and chemical properties [1–6] in recent years. Specifically, its unique polyaromatic and planar structure as well as its high surface area allow highly efficient loading of aromatic anticancer drugs via $\pi-\pi$ stacking, making it an excellent platform for biomedical applications such as drug delivery [7, 8]. Incapability of biological dispersion remains a major issue impeding biologically relevant applications, although graphene oxide (GO) can be stable and well dispersed in pure water. Fast and serious aggregation would occur in media generally rich in salts or proteins, such as cell culture medium and serum,

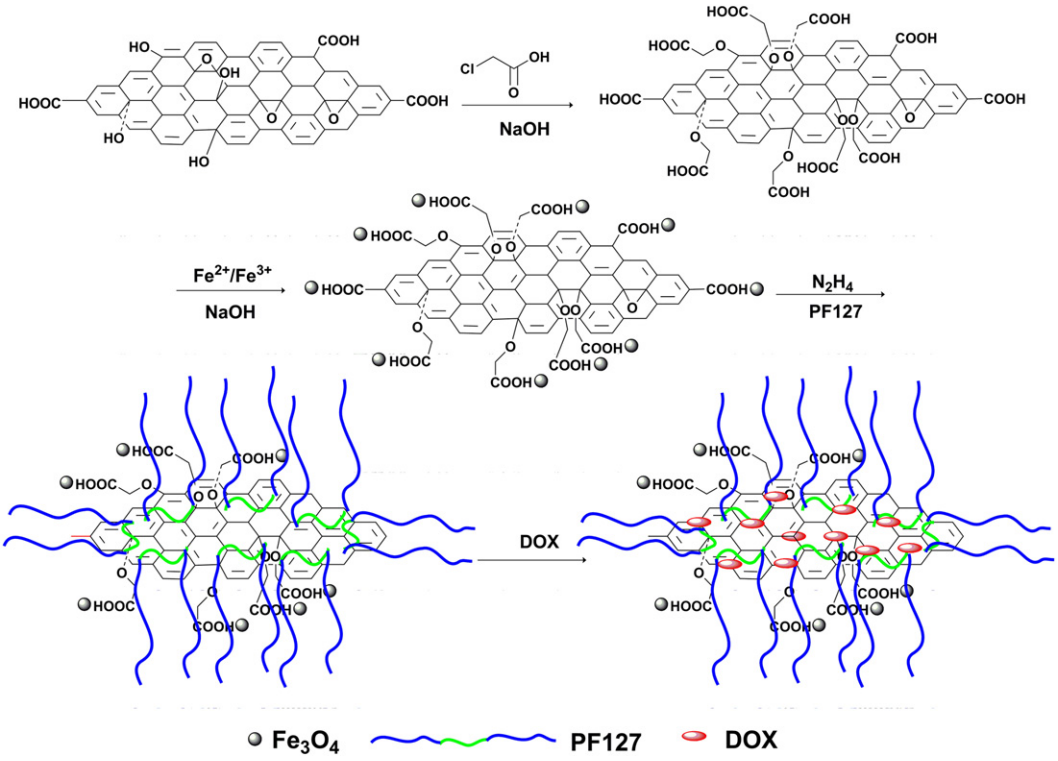

Scheme 1. Synthetic route of GO–COOH, GO–COOH/Fe_3O_4, GN/Fe_3O_4/PF127 and schematic illustration of DOX loading on GN/Fe_3O_4/PF127.

due to the screening effect of the electrostatic charges and nonspecific binding of proteins on them [9]. Various strategies have been developed to address this issue, including control of the distribution and density of electrostatic charges by regulating the C/O ratio during the oxidation process to obtain graphene oxide, or the use of an amphiphilic copolymer as a steric stabilizer, such as functionalized polyethylene glycol (PEG) [10, 11]. The latter method is commonly used to promote its electrostatic stability in electrolyte solution.

Liu *et al* carried out pioneering work by utilizing PEGylated graphene oxide (GO-PEG) as a nanocarrier to load water-insoluble anticancer drugs and evaluating its cytotoxicity to human cancer cells [9]. Since then, many functionalized graphene materials with excellent biocompatibility have been developed for DNA detection [12], cellular probing [13], gene therapy [8], photodynamic therapy [14, 15] and drug delivery [9]. Our group has successfully engineered a novel Pluronic F127/graphene nanohybrid for pH responsive drug delivery [16] and a GO based multifunctional nanocomposite for *in vitro* hepatocarcinoma diagnosis and treatment [17]. Currently, the engineering of multifunctional nanomaterials by graphene based systems for potential biomedical applications is being actively explored for future disease diagnosis and treatment.

Photothermal therapy (PTT) is known for its noninvasive medical technology to treat diseases such as cancer, which employs photo-absorbing agents to generate heat from optical energy, leading to the 'burning' of cancer cells [18]. In the past decade, PTT as a minimally invasive treatment methodology has aroused widespread interest. Graphene and its derivatives were found to exhibit considerable optical absorption in the near-infrared (NIR) region ideal for PTT [15]. This led to the recent work using GO-PEG for efficient photothermal ablation of tumors in animal experiments [19]. Liu *et al* designed a novel PEG functionalized graphene based probe for applications in multimodal imaging guided photothermal therapy of cancer [18]. Markovic *et al* also compared the photothermal anticancer activity of graphene nanosheets (GNs) and carbon nanotubes (CNTs). They concluded that GNs are distinctly more efficient than CNTs to induce photothermal death of U251 human glioma cells *in vitro* [20]. Magnetite (Fe_3O_4) nanoparticles have long been of scientific interest and widely used as a magnetic resonance contrast agent for magnetic resonance imaging (MRI) [21]. The combination of the individual advantages of GNs and Fe_3O_4 would show great potential in biomedical applications.

Herein, we developed a GN/Fe_3O_4/Pluronic F127 nanohybrid directed at chemophototherapy by combining the chemo and photothermal treatment via a one-pot process, in which the process includes simultaneous reduction of graphene oxide/Fe_3O_4 and subsequent assembly of PF127 onto GNs as shown in scheme 1. The presence of PF127 gives the GNs high aqueous solubility and stability in a physiological environment. This unique nanohybrid accommodates multiple functional components: the GNs possess photothermal properties; Fe_3O_4 can be used as an MRI agent; meanwhile, an anticancer drug (Doxorubicin) can be efficiently loaded onto the GNs via π–π interaction. As a result, this multifaceted nanohybrid is expected to be a promising platform to achieve simultaneous chemophototherapy and MRI.

2. Experimental details

2.1. Materials

Flake graphite was purchased from Shanghai Yifan Graphite Company (purity ≥99.9%); 98% sulfuric acid (H_2SO_4), 37% hydrochloric acid (HCl), 30% hydrogen peroxide (H_2O_2), sodium nitrate ($NaNO_3$), sodium persulfate ($Na_2S_2O_8$), phosphorus pentoxide (P_2O_5), potassium permanganate ($KMnO_4$), sodium hydroxide (NaOH), ferric chloride hexahydrate ($FeCl_3 \cdot 6H_2O$), ferrous chloride tetrahydrate ($FeCl_2 \cdot 4H_2O$) and chloroacetic acid ($CH_2ClCOOH$) were all analytical reagents purchased from Shanghai Chemical Reagent Company; Doxorubicin hydrochloride (DOX · HCl) was purchased from Zhejiang Hisun Pharmaceutical Company; the triblock copolymer PF127 (PEO_{99}–PPO_{67}–PEO_{99}) was purchased from Sigma Aldrich. The dialysis membrane with a molecular weight cutoff of 8000–12 000 g mol^{-1} was purchased from Spectrum Laboratories. WST-1 cell proliferation and cytotoxicity assay kits were purchased from Beyotime Institute of Biotechnology. All other chemicals were obtained from Sinopharm Chemical Reagent Company as analytical grade and were used as received.

2.2. Preparation of GO

GO was prepared by a modified Hummers method [22]. In brief, 1.0 g of natural flake graphite, 0.5 g of $Na_2S_2O_8$ and 5.0 ml of 98% H_2SO_4 were mixed and reacted under stirring at 60 °C for 6 h, followed by exhaustive washing with double deionized (DD) water to obtain the pre-oxidized GO. The pre-oxidized GO was combined with 100 ml of 98% H_2SO_4 and 3.0 g of $KMnO_4$ gradually over 10 min in an ice water bath under continuous stirring. The mixture was then vigorously stirred at 35 °C for five days. Afterwards, 100 ml of DD water was added and kept for a further 15 min, 5.0 ml of 30% H_2O_2 was added to terminate the reaction. To remove ions of the oxidant and other inorganic impurities, the mixture was subjected to a repeated process of washing and centrifugation cycles. Tthe thus obtained GO aqueous dispersion was treated by ultrasonication (2 h, 600 W) to exfoliate the GO into small pieces, followed by centrifugation at 13 000 r min^{-1} to remove larger sized GO and the final collection of the nanoscaled GO.

2.3. Fabrication of GO–COOH/Fe_3O_4 nanohybrid via chemical deposition

The fabrication protocol of the nanohybrid was described in previously reported work [23–25]. Specifically, carboxylic acid groups were first introduced to the GO by reaction with chloroacetic acid according to our previous work [14]. Then, the GO–COOH (40 mg) was dissolved in 100 ml of NaOH (pH = 12) solution and sonicated at 600 W for 2 h to transform the carboxylic acid groups to carboxylate anions, followed by exhaustive dialysis. The solution was condensed to 40 ml, into which a solution of $FeCl_3 \cdot 6H_2O$ (800 mg) and $FeCl_2 \cdot 4H_2O$ (400 mg) in water (5.0 ml) was added. The mixture was stirred overnight under nitrogen (N_2) protection for the growth of Fe_3O_4 nanoparticles. After a repeated process of washing and centrifugation cycles, the solid product was re-dispersed in 30 ml of water and NaOH (4.0 ml, 3 mol l^{-1}) was added; the mixture was kept stirred at 65 °C for a further 2 h under a N_2 atmosphere. Then the mixture was dialyzed against water with timely refreshment of the water.

2.4. Construction of the GN/Fe_3O_4/PF127 hybrid

PF127 is an amphiphilic polymer, which was used to give the GN aqueous solubility and stability in a physiological environment [16]. 400 mg of PF127 was added to 15 ml of GO–COOH/Fe_3O_4 aqueous suspension (1.0 mg ml^{-1}) and the mixture was stirred for 30 min at room temperature. Then 400 μl of hydrazine monohydrate was added and the mixture was stirred continuously at 40 °C for 24 h under sonication to reduce the GO to GNs. The solution was dialyzed against DD water to remove the hydrazine monohydrate, followed by magnetic separation to remove the unattached copolymer to yield the GN/Fe_3O_4/PF127 nanohybrid.

2.5. DOX loading onto the GN/Fe_3O_4/PF127 nanohybrid

The process of DOX loading onto the GN/Fe_3O_4/PF127 nanohybrid was as follows: a predetermined concentration (0.1, 0.2, 0.3, 0.5, 0.8 or 1.0 mg ml^{-1}) of DOX · HCl was stirred in the dark for 1 h with 10 ml of aqueous dispersion of GN/Fe_3O_4/PF127. The mixture was then subjected to sonication for 0.5 h, followed by stirring overnight at pH 8 in the dark. The excess DOX was removed via magnetic separation and exhaustively washed with DD water. The content of loaded DOX was obtained by subtracting the unloaded DOX from the initial amount of DOX. The drug encapsulation efficiency (DEE) of DOX on the nanohybrid was calculated from the following formula:

$$\text{DEE (w/w\%)} = (\text{weight of loaded drug/weight of nanohybrid}) \times 100\%.$$

2.6. Release behavior of DOX from the GN/Fe_3O_4/PF127 nanohybrid

The release behavior of DOX from the GN/Fe_3O_4/PF127 nanohybrid was investigated at 37 °C in saline buffer solutions with different pH values. Briefly, GN/Fe_3O_4/PF127/DOX samples (1.5 ml) with different pH (5 or 7) media were placed into centrifuge tubes and mounted into a shaking bed at 37 °C with a rotation speed of 150 rpm. To monitor the release behavior, samples were periodically taken out at desired time intervals and subjected to centrifugation at 13 000 rpm. The DOX concentration in the supernatant was analyzed using a UV/vis spectrophotometer by its absorbance at 480 nm and estimated by a standard DOX concentration curve generated from a series of DOX solutions with various concentrations. The amount of DOX released from the GN/Fe_3O_4/PF127 was the amount of DOX in the supernatant.

2.7. In vitro photothermal treatment and cytotoxicity assay

The cytotoxicities of GN/Fe_3O_4/PF127 and GN/Fe_3O_4/PF127/DOX were evaluated by using a WST-1 cell proliferation and cytotoxicity assay kit. Briefly, HeLa cells were cultured in 96-well plates (5000 cells/well) using DMEM culture medium supplemented with 10% fetal bovine serum and 0.1% penicillin–streptomycin (150 μl) and incubated at 37 °C for 24 h. The medium in each well was then replaced with DMEM (150 μl) containing different concentrations of GN/Fe_3O_4/PF127 and GN/Fe_3O_4/PF127/DOX. After incubation for 1 h [15], cells were irradiated using a 660 nm laser at a power density of 0.5 W cm^{-2} for 15 min, whereas the control groups were just cells incubated with DMEM without added material. After a further 4 h incubation, WST-1 solution (10 μl) was added to each well followed by incubation for 4 h at 37 °C which allowed viable cells to reduce the WST-1 into orange formazan crystals. The plate was read at 450 nm on a Bio-Rad microplate reader for estimation of the cell viability (Thermo Fisher Scientific, Waltham, MA, USA).

The relative cell viability (%) was calculated by the following equation: cell viability = $(OD_{treated}/OD_{control}) \times 100\%$, where $OD_{treated}$ (OD = optical density) was obtained by comparing the OD with that of control wells containing only cell culture medium. Data were presented as the average (SD, $n = 5$).

2.8. MRI test

GN/Fe_3O_4/PF127 aqueous solutions with different concentrations (1.0, 0.5, 0.25, 0.125 mg ml^{-1}) were put into 1.5 ml centrifuge tubes. MRI scans of these samples were collected by a Siemens Verio 3.0 T MRI system (T_2-weighted image, TR: 4000 ms, TE : 900 ms, FOV: 199 × 199).

2.9. Laser scanning confocal microscope observation

HeLa cells were seeded in a six-well plate at a density of 1×10^5cells/well with complete medium. The cells were incubated for 24 h in a humidified atmosphere with 5% CO_2 at 37 °C. The cells were washed with PBS and incubated at 37 °C for 24 h with GN/Fe_3O_4/PF127/DOX of a certain concentration in complete DMEM. The cells were then irradiated by a 660 nm laser at a power density of 0.5 W cm^{-2} for 15 min, followed by twice washing the cells with PBS. The cells were fixed with 4% formaldehyde before observation. DAPI was employed to stain the cell nuclei for 10 min and then they were washed with PBS to remove the excess dye. The slides were mounted and observed with a laser scanning confocal microscope (Olympus, FV300, IX71, Tokyo, Japan).

2.10. Flow cytometric analysis (FCAS)

For FCAS analysis, HeLa cells (1×10^5 cells/well) were seeded into six-well plates and incubated for 24 h. After removal of the culture medium by PBS, the cells were incubated at 37 °C for 24 h with GN/Fe_3O_4/PF127 and GN/Fe_3O_4/PF127/DOX at a predetermined concentration in complete DMEM. Then the cells were irradiated by a 660 nm laser at a power density of 0.5 W cm^{-2} for 15 min. Thereafter, the cells were washed with PBS twice and harvested, then suspended in paraformaldehyde (500 μl, 2%) for FCAS analysis using an FCAS-Calibur flow cytometer (BD Biosciences, USA).

2.11. Measurements

A Tensor 27 FTIR spectrometer (Bruker AXS, China) was used to record the Fourier transform infrared (FTIR) spectra of powdered samples. The morphology of the resulting nanohybrids was observed by H7100 TEM at an acceleration voltage of 100 kV. Atomic force microscope (AFM) images of samples deposited on a freshly cleaved silicon surface were observed in the tapping mode with an SPA-300HV instrument. The size distribution and zeta-potential of the nanohybrids were determined using a Nano-ZS 90 Nanosizer (Malvern Instruments Ltd, Worcestershire, UK). UV/vis detection and fluorescence spectra were obtained with an ultraviolet/visible spectrophotometer (Varian, Hong Kong) and a Hitachi F2500 luminescence spectrometer (Hitachi, Hong Kong), respectively. Thermogravimetric analysis (TGA) was performed on a Pyris Diamond TG/DTA; the thermograms of freeze-dried samples covered the temperature range from room temperature to 800 °C at a scanning rate of 5 °C min^{-1}.

3. Results and discussion

3.1. Synthesis and structural characterization of the nanohybrids

GO was synthesized by a modified Hummers method with the size controlled by the oxidation conditions: the power and time of the subsequent ultrasound. A process of carboxylation was performed to convert the hydroxyl groups of GO into carboxyl groups which facilitated the following growth of Fe_3O_4. The superparamagnetic GO–COOH/Fe_3O_4 was then generated via a chemical precipitation of iron ions on the surface of the carboxylated GO. Finally, the GN/Fe_3O_4/PF127 nanohybrid was prepared via a one-pot process with simultaneous reduction of GO and self-assembly of PF127 with GNs to yield the PF127 functionalized GN/Fe_3O_4 nanohybrid (scheme 1). An optimized ratio of $FeCl_3$:$FeCl_2$:GO = 20:10:1 (W/W) was implemented to maximize the Fe_3O_4 content of the nanohybrid while affording reasonable stability. PF127 was chosen as the stabilizing agent because of its amphiphilic nature and excellent biocompatibility. The amphiphilic nature of PF127 can promote stability of the GNs through hydrophobic interaction, and its biocompatibility will be favorable for biomedical applications [26]. Zeta-potential test was used to track the process of the synthesis, as the content of the carboxyl groups varies among different derivatives. The zeta-potential of GO–COOH (−36 mV) is found to be more negative compared with that before carboxylation (−32 mV). A further dramatic increase for GN/Fe_3O_4/PF127 was observed after Fe_3O_4 deposition. These alterations indicate the successful synthesis of carboxylation and reduction of GO.

FTIR (figure 1) and UV/vis (figure 2) spectra were obtained to trace the structural changes during the chemical

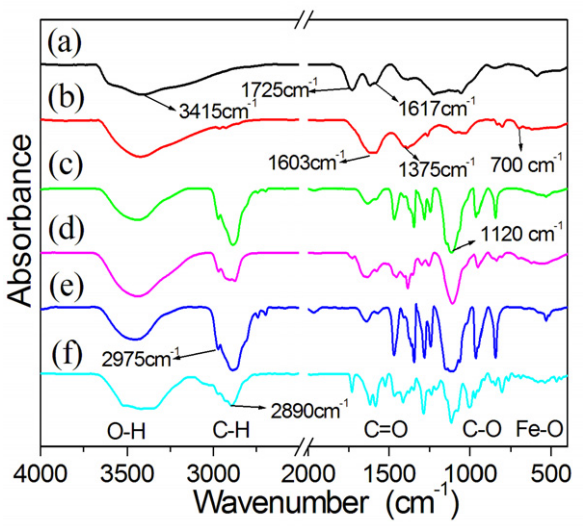

Figure 1. FTIR spectra of (a) GO, (b) GO–COOH/Fe_3O_4, (c) GN/Fe_3O_4/PF127, (d) GN/Fe_3O_4/PF127/DOX, (e) PF127 and (f) DOX.

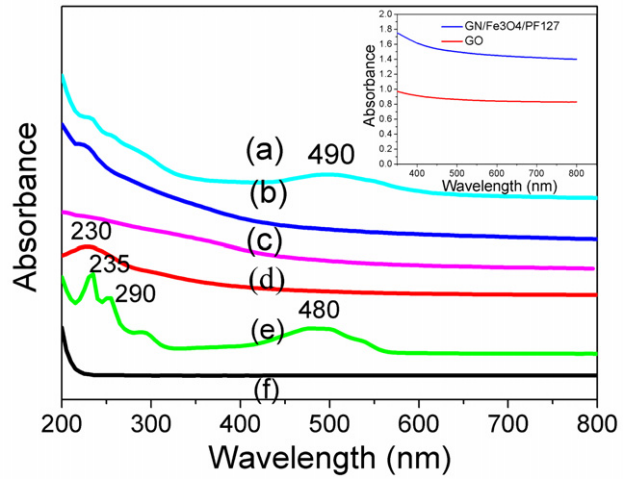

Figure 2. UV spectra of (a) GN/Fe_3O_4/PF127/DOX, (b) GN/Fe_3O_4/PF127, (c) GO–COOH/Fe_3O_4, (d) GO, (e) DOX and (f) PF127. The inset shows the spectra of GN/Fe_3O_4/PF127 and GO in the range of 350–800 nm.

process to yield the nanohybrid. In the FTIR spectra of GO–COOH/Fe_3O_4, the absorption peak of C=O for GO at 1725 cm^{-1} shifts to 1603 cm^{-1}, ascribed to the coordination interaction of –COOH with Fe^{3+} and Fe^{2+} ions, while the characteristic stretching vibration peak of the Fe–O bond generally located at 570 cm^{-1} shifts to a higher wavelength of 700 cm^{-1} [24, 27]. After PF127 conjugation, the characteristic peaks at 2975 cm^{-1} and 2890 cm^{-1} belonging to $–CH_3$ and $–CH_2$ groups, respectively, were observed, indicating the presence of PF127.

The UV spectra also reveal the structural change during the fabrication process of the nanohybrid (figure 2). A typical peak at 230 nm associated with conjugated planar structure was observed for GO (figure 2(d)), whereas it was largely reduced and broadened after being complexed with Fe_3O_4 (figure 2(c)). A strong van der Waals force during the coordination is believed to weaken the ultraviolet absorption ability of GO [28].

The composition of the nanohybrid was analyzed by the thermal decomposition behavior of the samples in an inert atmosphere, as shown in figure S1. For GO, there are three major mass losses with temperature increase in the TGA curves: (i) an initial approximately 5% weight loss below 100 °C corresponding to water evaporation; (ii) then two stages of weight loss occur around 150–400 °C mainly due to pyrolysis of the labile oxygen containing functional groups at different positions on the GO; (iii) the mass loss above 400 °C attributed to bulk pyrolysis of the carbon skeleton. In contrast, GO–COOH/Fe_3O_4 shows a different weight loss behavior below 400 °C, which might be due to the carboxylation effects on GO. Meanwhile, a prominent weight loss (19%) with an onset of 682 °C was observed, attributable to breakdown of the –COOH groups coordinated with Fe_3O_4 nanoparticles in the GO–COOH/Fe_3O_4 hybrid [29]. Importantly, the TGA curves of the GO–COOH/Fe_3O_4 hybrid show a higher end residue (ca. 40%) compared to GO (ca. 37%), indicating that the Fe_3O_4 incorporation affected the stability of the GO. To calculate the weight ratio of the two compounds, Fe_3O_4 nanoparticles were dissolved using diluted hydrogen chloride for a certain amount of GO/Fe_3O_4 composite. A dialysis process was conducted to remove salts followed by a freeze-drying process to collect GO. Thus, the weight ratio of GO and Fe_3O_4 content in the composite could be calculated and was found to be around 2:1. Differently from the GO and the GO–COOH/Fe_3O_4 hybrid, the weight loss behavior of GN/Fe_3O_4/PF127 does not exhibit a similar trend. After a minor weight loss at the initial stage, a remarkably high weight loss (91%) in a relatively narrow temperature range (350–440 °C) takes place, which is mainly attributable to decomposition of PF127. This result indicates a predominant weight ratio of PF127 in the nanohybrid. The inherent high-surface-area property of graphene was believed to contribute such a high capacity of PF 127 conjugation.

3.2. Morphology study

TEM, AFM and DLS were used to characterize the size and morphology of the GO, GO–COOH/Fe_3O_4 and GN/Fe_3O_4/PF127 nanohybrid. TEM images (figure 3) show that the GO is well dispersed and the average lateral size is around 80 nm. After deposition with Fe_3O_4, the lateral size becomes a little larger (∼110 nm). Dots with obviously higher contrast are observed to be distributed on the GO surface in the GO–COOH/Fe_3O_4 and GN/Fe_3O_4/PF127 nanohybrid, indicating the existence of Fe_3O_4. A comparable size but an obscure boundary was observed in the TEM image of GN/Fe_3O_4/PF127, which might be due to the relatively low contrast of PF127 copolymer compared with that of graphene and Fe_3O_4 nanoparticles. High resolution TEM imaging of the iron oxide in the nanohybrid is provided in the supporting information (figure S2 available at stacks.iop.org/Nano/25/065602/mmedia). The magnified fringe spacing of Fe_3O_4 nanoparticles is found to be 0.29 nm, which agrees with the lattice spacing of the (220) plane in Fe_3O_4 with crystalline phase [30]. AFM images provide more direct and solid information to reveal the microstructures.

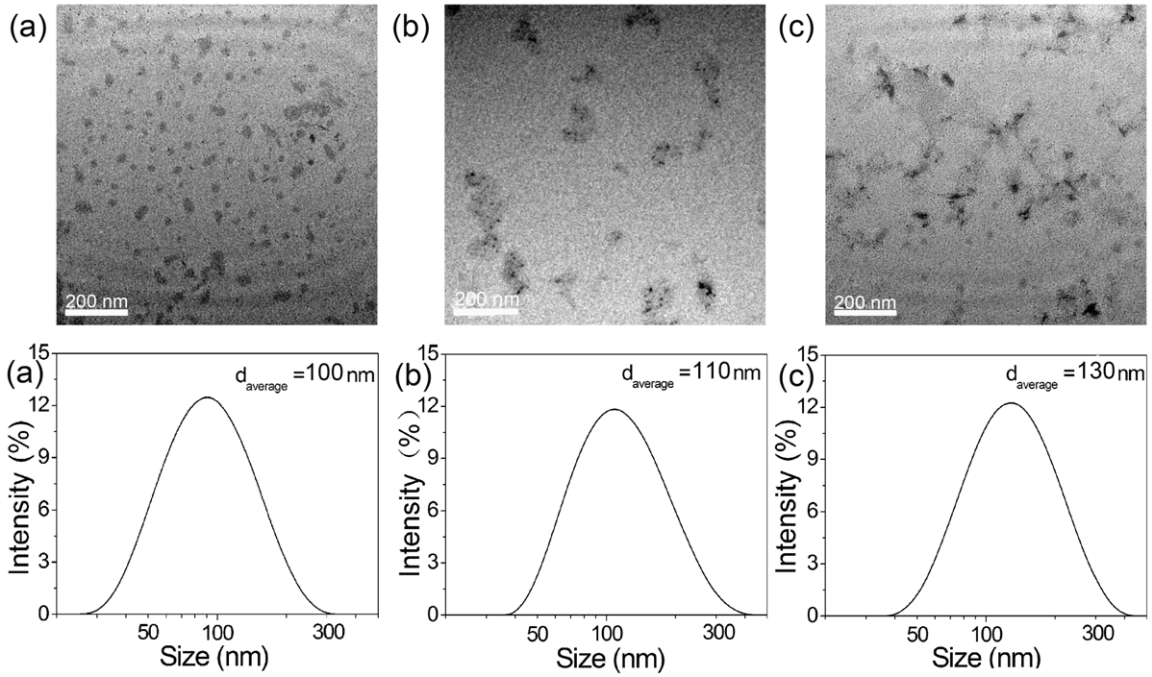

Figure 3. TEM image (top) and size distribution (bottom) of (a) GO, (b) GO–COOH/Fe_3O_4 and (c) GN/ Fe_3O_4/PF127.

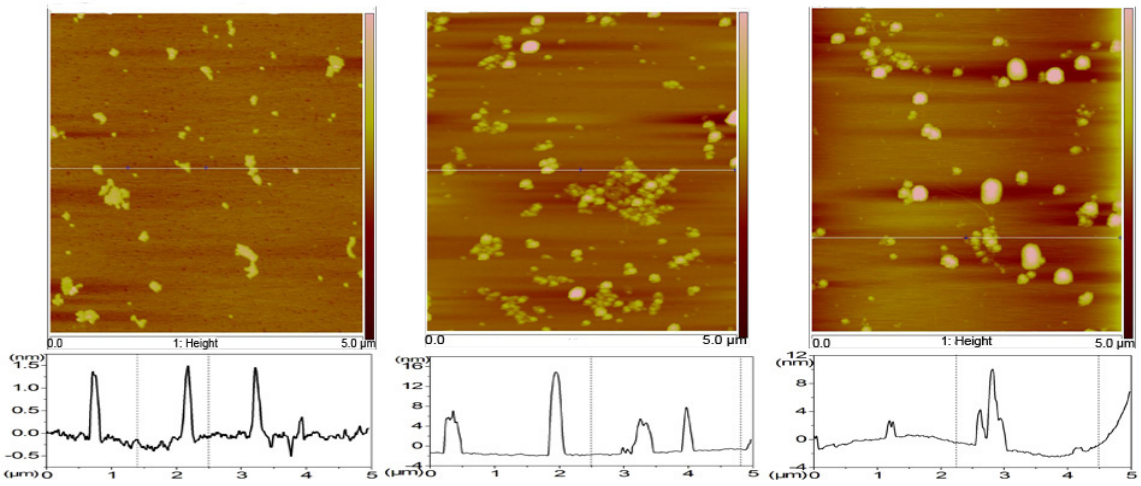

Figure 4. Tapping mode AFM images of GO (left), GO–COOH/Fe_3O_4 (middle) and GN/Fe_3O_4/PF127 (right).

As shown in figure 4, the average thickness of around 1.0 nm suggests single or several layers for the GO sheet [31]. Whereas the incorporation of Fe_3O_4 leads to a sharp increase in thickness (10 nm) of the GO–COOH/Fe_3O_4 and hybrid, the above results suggests that the introduction of Fe_3O_4 dramatically increases the thickness of the hybrid but without obvious effect on the width.

3.3. Physiological stability

Physiological stability is a pivotal and prerequisite factor to meet the requirements for biomedical applications. Thus PBS buffer saline and cell medium (DMEM) with fetal bovine serum (FBS) solutions were used to preliminarily evaluate the biological stability of the GN/Fe_3O_4/PF127 nanohybrid. GO exhibits high dispersivity and stability in water, but undergoes fast aggregation in both PBS and DMEM with FBS (figure S3 available at stacks.iop.org/Nano/25/065602/mmedia). In sharp contrast, GN/Fe_3O_4/PF127 keeps high stability when incubated with the same test solution. The significant improvement in stability is mainly attributed to PF127 complexation, in which hydrophobic poly(propylene oxide) (PPO) segments can bind to the hydrophobic surface of graphene via the hydrophobic effect while the hydrophilic poly(ethylene oxide) (PEO) chains extend into the water. This unique interface would suppress the appearance of aggregation phenomena to

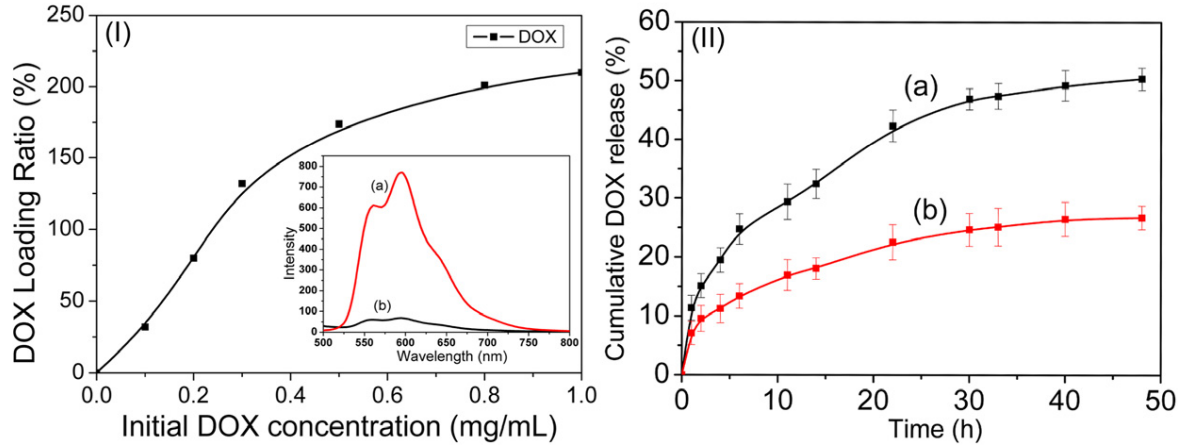

Figure 5. (I) Loading capacity of DOX on GN/Fe_3O_4/PF127 at different initial DOX concentrations. The insets are the fluorescence spectra of (a) DOX and (b) GN/Fe_3O_4/PF127/DOX in water at 480 nm excitation wavelength; the concentration of DOX in both (a) and (b) is 10 μg ml^{-1}. (II) The release behavior of DOX from GN/Fe_3O_4/PF127 at different pH values: (a) pH = 5, (b) pH = 7.

achieve high biological stability, which is highly favorable for future animal study.

3.4. Drug loading and release behavior

The antitumor drug DOX with inherent fluorescence properties was chosen to assess the drug loading capability of the GN/Fe_3O_4/PF127 nanohybrid. The loading process can be easily traced by fluorometer, taking advantage of the quenching effect of graphene due to the energy transfer induced by π–π interaction. Being excited at 480 nm, the fluorescence emission spectra of DOX have maximum intensity at 593 nm (figure 5(I) inserts). Once loaded onto GN/Fe_3O_4/PF127, the fluorescence intensity dramatically decreases due to the fluorescence quenching effect. In addition, the characteristic absorption peak of DOX at 480 nm red shifts to 490 nm in the UV/vis spectrum (figure 2(e)), which is due to the ground-state electron donor–acceptor interaction between the two components. The above data clearly support the successful loading of DOX onto the GN/Fe_3O_4/PF127 hybrid.

The DOX encapsulation efficiency of GN/Fe_3O_4/PF127 as a function of DOX dosage is summarized in figure 5(I). It is shown that the encapsulation efficiency of the GN/Fe_3O_4/PF127 increases as a function of DOX dosage and can reach as high as 210% (W/W) at a DOX concentration of 1.0 mg ml^{-1}. This encapsulation efficiency is higher than those of most existing drug carriers, such as carbon nanotubes and polymer vesicles, which are usually below 100% at saturated loading efficiency [10, 32–34].

Cancerous tissue is generally characterized by a lower pH than normal tissue. Thus, there has been intensive work on designing pH responsive delivery systems to take advantage of this biological discrepancy. The DOX release behavior from GN/Fe_3O_4/PF127 under different pH values was investigated. As shown in figure 5(II), DOX releases rapidly at the initial stage (<3 h), subsequently maintaining a moderate release rate. DOX shows a pH responsive release behavior in an acidic medium; an obviously faster release rate was found at pH 5.0. The facts of a stronger hydrogen-bonding interaction in neutral conditions and higher solubility of DOX under acidic conditions contribute to the above drug release discrepancy [34]. This pH-dependent drug release mechanism can accelerate the intracellular release due to the acidic microenvironments of intracellular lysosomes and endosomes.

3.5. Photothermal and magnetic properties

Graphene and its derivatives have been found to show considerable optical absorption in the near-infrared (NIR) region (as shown in figure 2, insets), which is favorable for applications of photothermal therapy [35–37]. To preliminarily investigate the photothermal properties of the GN/Fe_3O_4/PF127 nanohybrid, in this study, a 660 nm laser with a power of 0.5 W cm^{-2} was employed to irradiate the nanohybrid aqueous dispersion. The temperature of the dispersion with time of exposure was recorded with deionized water used as a control (figure 6). The curve plotted for temperature versus time of exposure shows that a fast increase in the temperature of the nanohybrid dispersion occurs during the first 15 min, i.e. from 25.6 to 35.7 °C, whereas the temperature of pure water exhibits a negligible change, which indicates the photothermal effect of the GN/Fe_3O_4/PF127 nanohybrid. Additionally, the upper limit temperature of the nanohybrid can be conveniently tuned by different factors (i.e. the concentration of the composite, the weight ratio of GN/Fe_3O_4 in the composite).

In addition, Fe_3O_4 based materials usually display magnetic effects upon exposure to a magnetic field. As expected, both GO–COOH/Fe_3O_4 and the GN/Fe_3O_4/PF127 nanohybrid can be easily anchored under magnetic field (insets in figure 6). Magnetic nanoparticles are popularly investigated to be used in MRI for diagnosis of cancer, which inspired us to further investigate the MRI function of GN/Fe_3O_4/PF127 nanohybrids. Using a 3.0 T medical superconducting MRI system, the T_2 relative signal intensity of GN/Fe_3O_4/PF127 (figure 7) was detected. As shown in the image, more darkened signals were observed for the GN/Fe_3O_4/PF127 nanohybrids compared with water, and the signal became darker with increase of concentration. The results indicate that GN/Fe_3O_4/PF127 can be a potential MRI contrast agent for diagnosis.

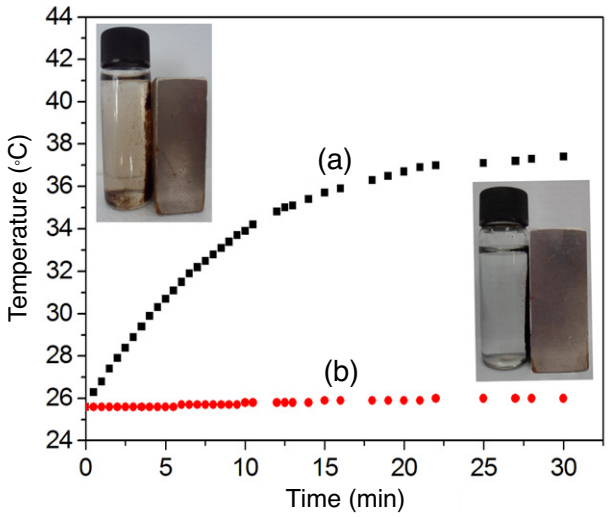

Figure 6. The photothermal effect of (a) GN/Fe_3O_4/PF127 (5 mg ml^{-1}) and (b) deionized water. The insets are pictures of GO/Fe_3O_4 (top) and GN/Fe_3O_4/PF127 (bottom) in a magnetic field.

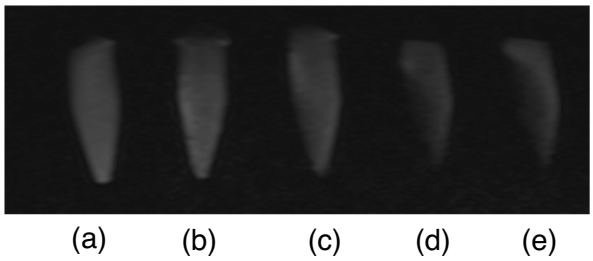

Figure 7. MRI images of GN/Fe_3O_4/PF127 aqueous suspension with different concentrations: (a) 0 mg ml^{-1}, (b) 0.125 mg ml^{-1}, (c) 0.25 mg ml^{-1}, (d) 0.5 mg ml^{-1} and (e) 1.0 mg ml^{-1}.

3.6. Cell cytotoxicity

The cellular cytotoxicities of drug-free and drug-loaded GN/Fe_3O_4/PF127 against HeLa cells were investigated by WST assay. As shown in figure 8, no obvious cytotoxicity is observed for GN/Fe_3O_4/PF127 at different concentrations. Even under high concentrations of up to 1000 μg ml^{-1}, the cellular viability of HeLa cells still maintains a high level (85%). Compared with drug-free GN/Fe_3O_4/PF127, the cytotoxicity of GN/Fe_3O_4/PF127/DOX against HeLa cells is much more potent. The cell viability reduces with increase in the concentration of GN/Fe_3O_4/PF127/DOX. The cell viability decreases to as low as 17% at the highest concentration. In order to investigate the influence of the photothermal effect, cells with GN/Fe_3O_4/PF127 or GN/Fe_3O_4/PF127/DOX were irradiated by laser for 15 min. The cell viability drops obviously regardless of whether drug-free or drug-loaded GN/Fe_3O_4/PF127 is used, which shows the photothermal effect. The combined chemotherapeutic and photothermal effects would be very favorable for the treatment of tumor-bearing mice in future work.

As shown in figures 9 and 10, CLSM and FCAS were used to investigate the cellular uptake behavior of the GN/Fe_3O_4/

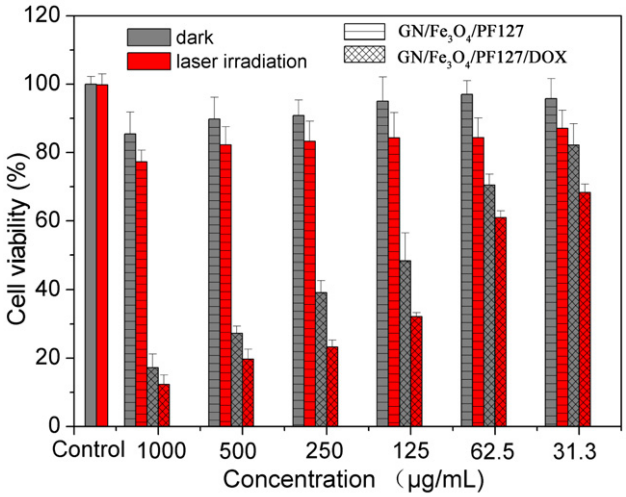

Figure 8. Cell proliferation of HeLa cells after 24 h incubation with different concentrations of GN/Fe_3O_4/PF127 and GN/Fe_3O_4/PF127 with or without laser irradiation. The red and gray colors indicate cells incubated with and without laser irradiation, respectively. (Irradiation conditions: 660 nm laser at a power density of 0.5 W cm^{-2} for 15 min.)

PF127/DOX against HeLa cells. It is critical for the DOX to be released from the GN/Fe_3O_4/PF127 and accumulate in the nucleus for anticancer activity via interaction with DNA [16, 38]. In the image of CLSM, obvious red fluorescence of DOX is detected in both the cytoplasm and the nucleus, especially in the nucleus of HeLa cells with or without irradiation, suggesting that DOX has been successfully uptaken by the HeLa cells. Consistently with the results of CLSM, FCAS shows that the uptake efficiencies of both samples exposed with or without irradiation are very high; the efficiencies of the samples are higher than 85%, indicating that most of the DOX released from the GN/Fe_3O_4/PF127 is internalized by the HeLa cells. The experimental results show that DOX can be released from GN/Fe_3O_4/PF127 and most of the DOX released from GN/Fe_3O_4/PF127 can be easily uptaken by HeLa cells.

4. Conclusions

In summary, multifunctional graphene based GN/Fe_3O_4/PF127 nanohybrid was engineered via a one-pot process including simultaneous reduction of GO–COOH/Fe_3O_4 assembly of PF127 onto graphene nanosheets (GNs). The nanohybrid exhibits high solution dispersivity and physiological stability, as well as high DOX encapsulation efficiency. Investigation of DOX release reveals a pH-dependent release manner with accelerated release in acidic conditions. Moreover, the GN/Fe_3O_4/PF127 nanohybrid exhibits a photothermal effect due to the considerable optical absorption in the near-infrared region of GNs. With the biological activity of DOX, cellular toxicity assays show a remarkable cytotoxicity of the DOX-loaded GN/Fe_3O_4/PF127 nanohybrid against HeLa cells. In combination with photoirradiation, the cytotoxic effect was intensified. CLSM and FCAS reveal that the nanohybrid can be easily uptaken into HeLa cells. This multifunctional graphene

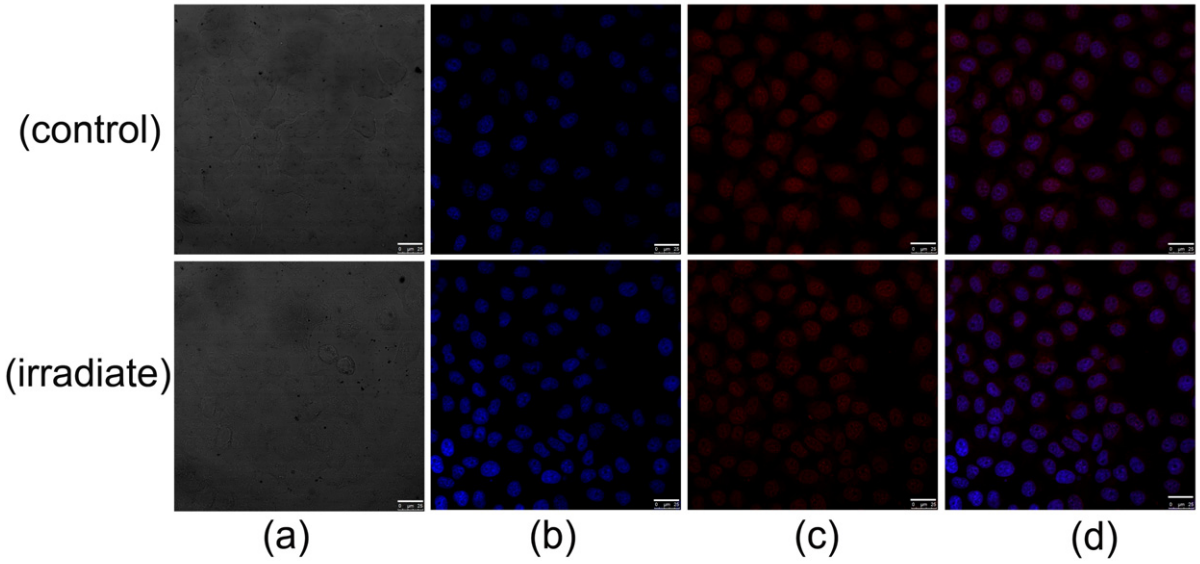

Figure 9. CLSM images of HeLa cells incubated with GN/Fe_3O_4/PF127/DOX: (a) bright field, (b) fluorescent image of DAPI, (c) fluorescent image of DOX and (d) merged image of (b) and (c). The concentration of both samples is 125 μg ml^{-1}. (The scale to represents 25 μm.)

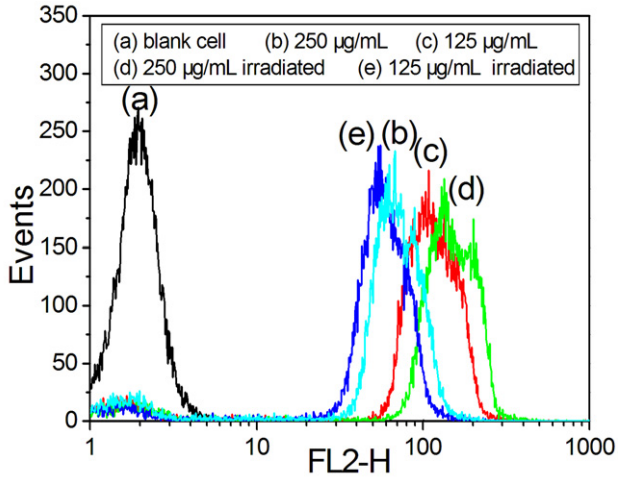

Figure 10. Flow cytometric analysis of HeLa cells which are untreated (a) or treated with different concentrations of GN/Fe_3O_4/PF127/DOX with ((d), (e)) or without ((b), (c)) irradiation; (b), (d) 250 μg ml^{-1} and (c), (e) 125 μg ml^{-1}.

based nanohybrid integrates simultaneous imaging, pharmaceutical functionalities and photothermal effects, showing promising prospects in biomedicine, biomaterial separation and diagnosis.

Acknowledgments

This work was financially supported by the 973 program (2013CB967500), the National Natural Science Foundation of China (21104059, 51173136 and 51073121), the Shanghai Rising-Star Program (12QA1403400), the 'Chen Guang' project supported by the Shanghai Municipal Education Commission and the Shanghai Education Development Foundation.

References

[1] Soldano C, Mahmood A and Dujardin E 2010 *Carbon* **48** 2127–50
[2] Kim T Y, Lee H W, Stoller M, Dreyer D R, Bielawski C W, Ruoff R S and Suh K S 2011 *ACS Nano* **5** 436–42
[3] Lu T, Pan L, Li H, Zhu G, Lv T, Liu X, Sun Z, Chen T and Chua D H C 2011 *J. Alloys Compounds* **509** 5488–92
[4] Wang H, Hao Q, Yang X, Lu L and Wang X 2010 *Nanoscale* **2** 2164–70
[5] Bai S and Shen X P 2010 *Prog. Chem.* **22** 2106–18
[6] Liu A, Li C, Bai H and Shi G 2010 *J. Phys. Chem.* C **114** 22783–9
[7] Guo Y, Guo S, Ren J, Zhai Y, Dong S and Wang E 2010 *ACS Nano* **4** 4001–10
[8] Zhang L, Lu Z, Zhao Q, Huang J, Shen H and Zhang Z 2011 *Small* **7** 460–4
[9] Liu Z, Robinson J T, Sun X and Dai H 2008 *J. Am. Chem. Soc.* **130** 10876–7
[10] Hong B J, An Z, Compton O C and Nguyen S T 2012 *Small* **8** 2469–76
[11] Hong B J, Compton O C, An Z, Eryazici I and Nguyen S T 2012 *ACS Nano* **6** 63–73
[12] Balapanuru J, Yang J X, Xiao S, Bao Q, Jahan M, Polavarapu L, Wei J, Xu Q H and Loh K P 2010 *Angew. Chem. Int. Edn* **49** 6549–53
[13] Yang X, Wang Y, Huang X, Ma Y, Huang Y, Yang R, Duan H and Chen Y 2011 *J. Mater. Chem.* **21** 3448–54
[14] Dong H Q, Zhao Z L, Wen H Y, Li Y Y, Guo F F, Shen A J, Frank P, Lin C and Shi D L 2010 *Sci. China-Chem.* **53** 2265–71
[15] Tian B, Wang C, Zhang S, Feng L and Liu Z 2011 *ACS Nano* **5** 7000–9

[16] Hu H, Yu J, Li Y, Zhao J and Dong H 2012 *J. Biomed. Mater. Res.* A **100A** 141–8
[17] Shen A J, Li D L, Cai X J, Dong C Y, Dong H Q, Wen H Y, Dai G H, Wang P J and Li Y Y 2012 *J. Biomed. Mater. Res.* A **100A** 2499–506
[18] Yang K, Hu L, Ma X, Ye S, Cheng L, Shi X, Li C, Li Y and Liu Z 2012 *Adv. Mater.* **24** 1868–72
[19] Zhang W, Guo Z, Huang D, Liu Z, Guo X and Zhong H 2011 *Biomaterials* **32** 8555–61
[20] Markovic Z M, Harhaji-Trajkovic L M, Todorovic-Markovic B M, Kepic D P, Arsikin K M, Jovanovic S P, Pantovic A C, Dramicanin M D and Trajkovic V S 2011 *Biomaterials* **32** 1121–9
[21] Cong H-P, He J-J, Lu Y and Yu S-H 2010 *Small* **6** 169–73
[22] Li Y and Wu Y 2009 *J. Am. Chem. Soc.* **131** 5851–7
[23] Yao Y, Miao S, Liu S, Ma L P, Sun H and Wang S 2012 *Chem. Eng. J.* **184** 326–32
[24] Yang X, Zhang X, Ma Y, Huang Y, Wang Y and Chen Y 2009 *J. Mater. Chem.* **19** 2710–4
[25] Kassaee M Z, Motamedi E and Majdi M 2011 *Chem. Eng. J.* **172** 540–9
[26] Chiappetta D A and Sosnik A 2007 *Eur. J. Pharm. Biopharm.* **66** 303–17
[27] Chin S F, Iyer K S and Raston C L 2008 *Lab Chip* **8** 439–42
[28] Murakami H, Nomura T and Nakashima N 2003 *Chem. Phys. Lett.* **378** 481–5
[29] Huang J, Wan S, Guo M and Yan H 2006 *J. Mater. Chem.* **16** 4535–41
[30] Yan H, Zhang J C, You C X, Song Z W, Yu B W and Shen Y 2009 *Mater. Chem. Phys.* **113** 46–52
[31] Lubbe A S, Bergemann C, Huhnt W, Fricke T, Riess H, Brock J W and Huhn D 1996 *Cancer Res.* **56** 4694–701
[32] Batrakova E V and Kabanov A V 2008 *J. Control Release* **130** 98–106
[33] Reul R, Renette T, Bege N and Kissel T 2011 *Int. J. Pharm.* **407** 190–6
[34] Yang X, Zhang X, Liu Z, Ma Y, Huang Y and Chen Y 2008 *J. Phys. Chem.* C **112** 17554–8
[35] Kim H, Lee D, Kim J, Kim T I and Kim W J 2013 *ACS Nano* **7** 6735–46
[36] Robinson J T, Tabakman S M, Liang Y Y, Wang H L, Casalongue H S, Vinh D and Dai H J 2011 *J. Am. Chem. Soc.* **133** 6825–31
[37] Yang K, Zhang S, Zhang G X, Sun X M, Lee S T and Liu Z 2010 *Nano Lett.* **10** 3318–23
[38] Gewirtz D A 1999 *Biochem. Pharmacol.* **57** 727–41